Perisomatic Synaptic Targeting by Cholecystokinin-Basket Interneurons through NrCAM and Ankyrin B

Erik N. Oldre, Barrett D. Webb, Justin E. Sperringer, and Patricia F. Maness*

Department of Biochemistry and Biophysics, CB 7260

University of North Carolina School of Medicine

Chapel Hill, NC 27599

*corresponding author

srclab@med.unc.edu

919-428-0942

Key words: synapse, cell adhesion, NrCAM, Ankyrin, cholecytokinin basket interneurons

ABSTRACT

The perisomatic region of cortical pyramidal neurons (PNs) integrates local and long-range inputs and regulates firing.This domain receives GABAergic inputs from cholecystokinin (CCK)- and parvalbumin (PV)-expressing basket cells (BCs) but how synaptic contacts are established is unclear. Neuron-glial related cell adhesion molecule (NrCAM) is a homophilic transmembrane protein that binds the scaffold protein Ankyrin B. Here we show that NrCAM and Ankyrin B mediate perisomatic synaptic contact between CCK-BCs and PNs in mouse prefrontal cortex (PFC). Immunolabeling of CCK-BC terminals for vesicular glutamate transporter-3 (VGlut3) or vesicular glutamate transporter (VGAT) revealed a significant decrease in CCK-BC synaptic puncta on PN soma in NrCAM-null mice, however no decrease in PV-BC puncta, or cell loss. VGlut3+ CCK-BC puncta were also decreased by Ankyrin B deletion from PNs in Nex1Cre-ERT2:Ank2$^{flox/flox}$:EGFP mice. A novel CCK-BC reporter mouse expressing tdTomato (tdT) at the Synuclein-γ (*Sncg*) locus showed NCAM localized to presynaptic Sncg+ CCK-BCs, as well as to postsynaptic PN soma of WT mice. Results implicate NrCAM homophilic interactions and Ankyrin B binding with development of inhibitory connectivity between CCK-BCs and excitatory neurons of the PFC.

1. Introduction

Establishment of a proper balance of excitatory and inhibitory (E/I) connectivity is achieved during synaptic development of cortical networks, and perturbation of this balance is implicated in neurodevelopmental disorders such as autism spectrum disorder (ASD) [1]. Pyramidal neurons (PNs) are the principal excitatory cells of the mammalian cerebral cortex. PNs transform synaptic inputs into action potentials that stimulate long- and short-range targets.The firing rates of PNs are tuned by GABAergic interneuron subtypes that form synapses at different subcellular domains. The perisomatic region of cortical PNs (soma, proximal dendrite, axon initial segment) is the key compartment for integrating diverse inputs and producing action potentials. GABAergic

interneurons that target this domain regulate firing and synchronization of a large array of PNs. The perisomatic domain of PNs receives almost exclusively GABAergic inputs derived from cholecystokinin (CCK)- and parvalbumin (PV)-expressing basket cells (BCs) [2, 3]. PV-BCs are fast spiking interneurons that regulate timing and oscillations important for PN synchrony, whereas CCK-BCs are regular spiking interneurons that restrain firing, impacting mood, emotion, and working memory retrieval [4-7]. The prefrontal cortex (PFC) has essential roles in integrating inputs within circuits that regulate cognitive and emotional behaviors [8-12]. CCK-BCs are particularly important in the PFC [13, 7]. Although much is known about PV-BCs [5], CCK-BC development and function are less well understood, in part due to lack of appropriate transgenic lines.

Neuron-glial related cell adhesion molecule (NrCAM) is a transmembrane glycoprotein of the L1 family, whose members mediate diverse aspects of neural development, including cell adhesion, neuronal process growth, dendritic spine remodeling, and synaptogenesis [14]. The extracellular region of NrCAM has six Ig-like domains and five fibronectin III (FN) repeats, which engage in *trans* homophilic adhesion between cells. NrCAM mediates pruning of excess dendritic spines and excitatory synapses that are initially overproduced during postnatal development [15, 16]. Accordingly, NrCAM-null mice exhibit elevated levels of excitatory synapses and increased frequency of excitatory neurotransmission in neocortical PNs [17]. However, inhibitory transmission has not been fully investigated in these mice. The conserved cytoplasmic domain of NrCAM reversibly engages Ankyrin B (AnkB), a spectrin-actin scaffold protein that is a high confidence ASD risk factor (SFARI Gene Database). AnkB is also known to localize the voltage gated sodium channel Nav1.2 to the PN dendritic membrane important for back-propagation of action potentials [18]. Genomic studies revealed that NrCAM variants are significantly associated with autism [19], while behavioral tests in NrCAM-null mice have demonstrated a reduction in learning and social behaviors relevant to autism [20].

An *in vivo* BioID-MS approach identified neuronal NrCAM in a proteome of inhibitory interneuron synapses from mouse brain using the GABAergic synaptic

organizer, gephyrin, as a bait protein [21]. A similar approach netted NrCAM in a proteome enriched for neuron-astrocyte junctions [22]. Depletion of NrCAM from astrocytes or neurons by CRISPR/Cas9 editing decreased inhibitory synapse formation in mouse visual cortex. Astrocytic NrCAM deletion increased the rise time of miniature inhibitory postsynaptic potentials (mIPSCs) suggesting that NrCAM may be more important for inhibitory control at perisomatic sites than at distal dendrites. It was proposed that NrCAM on astrocytes binds neuronal NrCAM at inhibitory postsynaptic sites to mediate synaptic organization but the interneuron cell type was not identified. These findings prompted us to examine whether NrCAM regulates the density of inhibitory synapses made by CCK- or PV-BCs onto cortical PNs. We focused on the medial prefrontal cortex (PFC), which includes the anterior cingulate, prelimbic, and infralimbic cortex, because of its essential role in social and cognitive behavior [8-12]. Layer 2/3 of the PFC was prioritized, because neurons in this layer are pivotal in integrating long and short range inputs important for these behaviors [23]. Here we demonstrate that NrCAM and AnkB promote perisomatic synaptogenesis by CCK-BCs, but not PV-BCs, onto PNs in the mouse PFC, implicating neuronal NrCAM interactions in development of inhibitory connectivity in the PFC.

2. Materials and Methods

2.1 Mice

NrCAM-null mutant mice on a mixed 129S6/SvEv^{Tac} x Swiss Webster (CFW) background [24] were maintained by heterozygous matings and bred for multiple generations onto C57Bl/6 mice [17]. WT and NrCAM homozygous-null littermates were used for experiments. Nex1Cre-ERT2: *Ank2*^{flox}: EGFP^{flox} (C57Bl/6) conditional mutant mice delete the Ankyrin 2 gene, *Ank2,* from cortical pyramidal neurons under control of endogenous Nex1 regulatory sequences induced by tamoxifen (TMX) [25]. The Nex1 promoter drives TMX-inducible Cre-ERT2 recombinase only in postmitotic PNs and not interneurons, oligodendroglia, astrocytes, or non-neural cells [26]. To generate a reporter mouse line expressing the dsRed variant tdTomato (tdT) in CCK-BCs, Synuclein-gamma

(Sncg)-IRES2-FlpO driver mice (JAX 034424; C57Bl/6) [27, 28] were intercrossed with Ai65F mice (frt-stop-tdTomato; JAX 032864). Sncg-IRES2-FlpO; Ai65F double heterozygotes for Sncg and tdT alleles were intercrossed to obtain double homozygotes. Offspring were genotyped by PCR and found to be present in Mendelian ratios. Mice were fertile and viable through at least postnatal day P150. All studies used WT and mutant mice balanced for sex. Mice were bred and maintained according to policies of the University of North Carolina Institutional Animal Care and Use Committee (IACUC; AAALAC Institutional Number: #329; ID# 18-073, 21-039) in accordance with NIH guidelines.

2.2 Immunofluorescence Staining and Antibodies

Mouse brains were harvested after pericardial perfusion with 4% paraformaldehyde (PFA) in phosphate buffered saline (PBS; NaCl 137 mM, KCl 2.7 mM, Na_2HPO_4 10 mM, KH_2PO_4 1.8 mM). In all experiments 3-5 mice per genotype were used. Coronal sections (40µm) through the prefrontal cortex (PFC) and hippocampus were cut with a Leica VT1200S vibratome, and stored at 4ºC in PBS with 0.02% sodium azide. Brain sections were placed in a 12-well dish, washed 3x10 min in PBS, then blocked and permeabilized for 1h in a solution of PBS, 10% normal donkey serum (Millipore Sigma 566460) or 5% normal donkey serum with 5% normal goat serum, and 0.3% Triton X-100 (CAS No. 9036-19-5). A second set of 3x10 min washes in PBS followed. The sections then incubated in primary antibody solution for 48h at 4ºC. Primary antibody solutions were prepared from in PBS, 0.3% Triton X-100, and 5% normal serum. The negative control well received 1 mL of this solution. Primary antibody solutions contained 1:100 mouse anti-VGluT3 antibody (Synaptic Systems 135211, 1mg/ml) and 1:100 rabbit anti-Math2/NeuroD6 antibody (Abcam 85824, 0.9mg/ml); 1:500 mouse anti-parvalbumin 3C9 antibody (Novus Biologicals NBP2-50038, 1mg/ml) and 1:200 mouse anti-VGluT3 antibody (Synaptic Systems 135211, 1mg/ml); or 1:2500 rabbit anti-NECAB1 antibody (Sigma HPA023629, 0.20mg/ml). Mouse monoclonal antibody to vesicular glutamate transporter (VGAT) was from Synaptic Systems (131 011.) NrCAM mouse

antibody (1:250) was from Biolegend (MMS-5267). Mouse monoclonal antibodies to synaptotagmin 2b (Syt2b; 1:500) were from the Zebrafish International Resource Center #ANZNP1. Rabbit anti-RFP antibody (Rockland 600-301-379S; 1:1000) and chicken anti-mCherry antibody (Aves Labs MC88697977; 1:250) were used to detect tdTomato.

Brain sections were incubated with primary antibodies at 4ºC for 48 hours then washed with PBS 5x10 min. Secondary antibody solutions were prepared in PBS and used at: 1:500 Alexa Fluor 555 donkey anti-mouse antibody (Invitrogen A32773); 1:1000 Alexa Fluor 488 donkey anti-rabbit antibody (Jackson Immunoresearch 711-545-152); 1:667 Alexa Fluor 488 donkey anti-mouse antibody (Invitrogen A32766TR); 1:500 Alexa Fluor 555 donkey anti-rabbit antibody (Invitrogen A31572); 1:1000 Alexa Fluor 647 donkey anti rabbit (Invitrogen 2181018); 1:1000 Alexa Fluor 488 goat anti-chicken (Invitrogen A32931TR). Sections were incubated at 4ºC with rocking for 2 hours, then washed 5x10 min with PBS. Sections were removed from wells and placed on Fisherbrand Superfrost Plus microscope slides (Cat. No. 12-550-15, 25 x 75 x 1 mm) with Corning High Precision No.1.5H coverslips (170 ± 5um, 24 x 50mm). Invitrogen Prolong Glass solution (2525808) was used to mount the coverslips. Slides were placed in the dark for 18 to 48 hours, then moved to 4ºC.

2.3 Imaging Acquisition and Analysis

Images used for quantitative analysis of puncta and soma, and for immunolocalization were taken with a Zeiss LSM 700 Confocal Laser Scanning Microscope at the UNC Microscopy Services Laboratory (Pablo Ariel, Director). Identical settings were used to capture images from WT and mutant brain sections. Images were acquired using a pinhole size of 1 AU with pixel sizes of 0.13-0.14 µm. Deconvolution of confocal images was performed utilizing AutoQuant 3 software (Media Cybernetics). Images were analyzed in FIJI. In all experiments 3-5 mice per genotype were used.

Coronal brain sections through PFC layer 2/3 were subjected to double immunofluorescence staining of presynaptic vGlut3 or Syt2b, and postsynaptic

Math2 or EGFP using Alexafluor-conjugated secondary antibodies. Perisomatic synaptic puncta were scored blind to observer on PN soma of WT and NrCAM-null mice, or on EGFP-expressing PNs in Nex1Cre-ERT2:RCE and Nex1Cre-ERT2: *Ank2* F/F: RCE mice. In replicate experiments puncta per soma measurements from 8-35 images per condition were scored blind to the observer in FIJI by scrolling through confocal z-stacks (0.3 µm optical sections) to fully capture the soma. The average number of puncta per soma was calculated for each image, and mean number of puncta per soma per genotype was calculated. Unpaired two-tailed t-tests or ANOVA with Tukey post hoc tests were performed using GraphPad Prism 9 to analyze statistically significant differences in means between genotypes ($p < 0.05$). Representative images represent maximum intensity projections where indicated through approximately 5 optical sections.

Immunofluorescence labeling of somal markers NECAB1 and Parvalbumin (Pv) was employed to quantify the density of CCK-BCs and Pv-BCs, respectively, in WT and NrCAM-null PFC and hippocampus. Images for quantitative analysis of soma were acquired with an Invitrogen EVOS M7000 Imaging System using 10x and 20x objectives. Labeled cells were scored manually, blind to observer, in multiple brain sections. Cell densities per unit area in each image were averaged across genotypes. Means were compared by two-tailed t-tests, $p < 0.05$.

3. Results

3.1 Perisomatic Synaptic Puncta of CCK-BCs on Pyramidal Neurons are Decreased in NrCAM-null Prefrontal Cortex.

NrCAM is expressed in layer 2/3 PNs in the cingulate region of the PFC [15] and in interneurons in mouse cortex [22]. A role for NrCAM in the formation of inhibitory CCK-BC synapses in the perisomatic domain of PNs in the PFC was evaluated by analyzing CCK-BC synaptic puncta in WT and NrCAM-null mice. CCK-positive, vasoactive intestinal peptide (VIP)-negative basket cells selectively express vesicular glutamate transporter 3 (VGluT3) at their presynaptic terminals [29], while PN soa express the transcription factor Math2/NeuroD6 in their soma.

Immunofluorescence staining of VGluT3-containing CCK-BC synapses on Math2+ PN soma showed a significant reduction in the mean number of perisomatic synapses of NrCAM-null PNs compared to WT PNs in adult mice (~P60) (Fig. 1 A,B; t-test = 0.01). Vesicular glutamate transporter (VGAT) is responsible for the uptake and storage of GABA by synaptic vesicles in multiple classes of interneurons. Immunofluorescence staining of VGAT-containing synaptic puncta on Math2+ PN soma showed a smaller but significant reduction in perisomatic synapses in NrCAM-null PFC compared to WT (Fig. 1 C,D; t-test, p = 0.02).

To control for possible CCK-BC loss caused by NrCAM deletion, which could account for the decreased number of VGlut3+ perisomatic synapses, antibodies directed against the somal marker N-terminal EF-hand calcium binding protein-1 (NECAB1) were used to immunolabel CCK-BC soma. NECAB1 is located in the nucleoplasm and cytosol of CCK-BCs in cortex and hippocampus, including VGlut3+/VIP- and VGlut3+/VIP+ interneurons, a subpopulation of PNs [30], and few PV-expressing interneurons [31]. Quantification of NECAB1-labeled soma showed that there was no significant difference in the mean density of these neurons in layer 2/3 of WT and NrCAM-null PFC (Fig. 1 E,F; p=0.99). These results suggested that the reduction of VGlut3+ perisomatic synaptic puncta on PNs in NrCAM-null PFC was not due to substantial loss of CCK-BCs.

3.2 Perisomatic Synaptic Puncta of Parvalbumin-Expressing Basket Cells are not Decreased in NrCAM-null Prefrontal Cortex.

CCK-BCs and PV-BCs are the major interneuron cell types that form perisomatic inhibitory synapses with PNs, and they can target the same PN [4]. Synaptotagmin-2b (Syt2b) is a synaptic vesicle protein involved in calcium-dependent neurotransmission that is a selective marker for PV-BC terminals [32]. To assess whether NrCAM plays a role in perisomatic targeting of PV-BC inputs to PNs, the number of PV-BC synaptic puncta was quantified in the perisomatic compartment of PNs by Syt2b and Math2 double immunofluorescence staining in

WT and NrCAM-null PFC (~P60). Quantitation of perisomatic puncta in layer 2/3 revealed no significant difference in the mean density of Syt2b+ synaptic puncta on Math2+ PN soma between WT and NrCAM-null PFC (Fig. 2 A,B; $p = 0.08$). This result indicated that PV-BC synaptic targeting to PN soma was not dependent on NrCAM.

CCK-BCs target not only PNs but to a lesser extent, the perisomatic compartment of PV-BCs, potentially causing disinhibition [33, 6]. Parvalbumin is predominantly localized to cell bodies of PV-BCs. To determine if NrCAM promotes CCK-BC synaptic connectivity with PV-BCs, the effect of NrCAM deletion on the number of VGlut3+ puncta onto PV-BC soma was analyzed. VGluT3- and PV-antibodies were used for double immunofluorescence staining of WT and NrCAM-null PFC. VGlut3+ puncta were quantified on PV+ soma in layer 2/3. Quantitation of double-labeled puncta revealed no significant difference in the mean density of CCK-BC synaptic puncta on PV-BC soma in WT compared to NrCAM-null PFC (Fig. 2 C,D; $p = 0.28$). These results indicated that NrCAM was not involved in the formation or maintenance of CCK-BC inputs to the perisomatic compartment of PV-BCs.

3.3 Postsynaptic Ankyrin B is Required for CCK-Basket Cell Targeting to Pyramidal Cell Soma

Ankyrins are important in stabilizing adhesion molecules, receptors, and ion channels at the neuronal cell surface [34]. For example, the AnkB binding site in the cytoplasmic domain of the neural adhesion molecule L1 was shown to be required for GABAergic synaptic targeting to PN soma [35]. Furthermore Ankyrin G was demonstrated to stabilize somatodendritic GABAergic synapses of cortical and hippocampal interneurons by preventing postsynaptic endocytosis of $GABA_A$ receptors [36]. We therefore asked whether postsynaptic AnkB on PNs mediated perisomatic targeting of CCK-BC synapses. We took advantage of Nex1Cre-ERT2: Ank2$^{flox/flox}$: EGFP^{flox} mutant mice, which can be induced to delete the Ankyrin 2 gene, *Ank2*, specifically from PNs by tamoxifen (TMX) treatment at P10-P13, simultaneously activating EGFP expression [25]. Nex1-Cre is activated only in postmitotic PNs and not in interneurons or glia [26]. Immunofluorescence

staining for VGlut3 showed a pronounced decrease in synaptic puncta on EGFP+ PN soma in PFC layer 2/3 of Nex1Cre-ERT2: Ank2$^{flox/flox}$: EGFP^{flox} mice compared to WT Nex1Cre-ERT2: Ank2$^{+/+}$: EGFP^{flox} mice (P60-P67), which had been treated with TMX at P10-P13 (Fig. 3 A,B; $p = 0.0.001$). There was no loss of cells identified by immunolabeling of the somal marker NECAB1 in WT compared to Ank2 mutant PFC (Fig. 3 C,D; $p=0.25$). Synaptic puncta on PN soma that are derived from PV-BC inputs can be visualized by immunostaining for synaptotagmin 2b (Syt2b). The density of Syt2B+ puncta on EGFP+ PN soma was unaltered by AnkB deletion in PNs (Fig. 3 E,F; $p = 0.99$).

3.4 Characterization of a Reporter Mouse Line for CCK-Basket Interneurons

To generate a reporter mouse line selective for CCK-BCs, we took advantage of recent findings that Synuclein-γ (Sncg) is selectively expressed by CCK-BCs but not PV-BCs, somatostatin (SST)- or non-CCK VIP-expressing interneurons [37, 38]. We produced a mouse expressing the fluorescent dsRed reporter tdTomato (tdT) at the Sncg genetic locus. To create this line, Sncg-IRES2-FlpO-neo mice (JAX 034434) were intercrossed with Ai65F mice (JAX 032864) containing the Rosa-CAG-Frt-STOP-Frt-tdT sequence. Expression of the recombinase enzyme FlpO in Sncg+ neurons was predicted to remove the STOP codon and induce tdT expression. Accordingly, adult brain sections (P60) of mice homozygous for both Sncg-IRES2-FlpO and tdT alleles were immunostained with anti-dsRed antibodies recognizing tdT, and AlexaFluor-555 secondary antibodies. Confocal imaging revealed labeled cells in the PFC, prominently in layer 2/3 (Fig. 4A), as well as other cortical areas including primary somatosensory and visual cortex (not shown). Control staining with secondary antibodies alone was negligible (Fig. 4B). tdT+ cells exhibited a neuronal morphology with labeled soma and emanating processes (Fig. 4C). Intrinsic tdT fluorescence was much lower but visible in neuronal soma and processes without dsRed antibody enhancement (Fig. 4D). CCK-BCs in the hippocampus are important in tuning network excitability [6, 39]. tdT-expressing cells in the Sncg-IRES2-tdT hippocampus after dsRed antibody labeling were evident in the stratum pyramidale (SP) of regions CA1, CA2, and CA3, with fewer

in the stratum oriens (SO), stratum radiatum (SR), and stratum lacunosum-moleculare (SLM) (Fig. 4E). tdT+ cells were also observed in the granule cell layer (GCL) and hilus (HI) of the dentate gyrus (DG) (Fig. 4E). Control staining with secondary antibodies alone was minimal (Fig. 4F), Higher magnification showed labeled soma and processes of neuronal cells in the SP (Fig. 4G). Intrinsic tdT fluorescence of SP neurons was lower but visible without antibody enhancement (Fig.4H).

To validate that the tdT reporter was expressed by CCK-BCs in the PFC, double immunostaining for tdT with anti-mCherry antibodies (recognizing tdT) and the somal marker NECAB1 was carried out in Sncg-IRES2-tdT brain sections (P60). Double labeled cells were observed in PFC layer 2/3 (Fig. 5). Quantitation indicated that a subset (~36%) of mCherry+ neurons co-expressed NECAB1. This value was in accord with other studies showing NECAB1 expression in CCK-BCs, and a subset of PNs and PV+ interneurons [31, 30]. We were unable to visualize mCherry colocalization with VGlut3 at perisomatic terminals in the Sncg-IRES2-tdT PFC, perhaps due to limited diffusion or transport of tdT in axons of labeled neurons. To further assess the specificity of tdT expression, double immunofluorescence staining was carried out in Sncg-IRES2-tdT brain sections with anti-PV and anti-dsRed antibodies (Fig. 5B). Quantitation of labeled cells in PFC layer 2/3 indicated that none of the PV+ neurons detectably expressed dsRed (Fig. 5B). Sncg-IRES2-tdT mice were also analyzed in a timecourse for tdT expression by immunofluorescence staining of the developing PFC (layer 2/3) in juvenile (P32-42) and adult (P60) mice (Fig. 5C,D). Cells expressing tdT showed a significant increase between P34 and P42, and between P34 and P60. The difference between P42 and P60 was negligible, indicating that expression remains constant during later stages of postnatal maturation. tdT+ cells were also present in this region at P21 (Fig. 6B).

In summary, the characterization of Sncg-IRES2-tdT cortex and hippocampus indicated that VGlut3+ CCK-BCs are selectively labeled, and that that PV-BCs do not express the tdT reporter.

3.5 NrCAM is Expressed by Presynaptic CCK-basket Interneurons and Postsynaptic Pyramidal Neurons in the Prefrontal Cortex

To determine if NrCAM was expressed at postsynaptic target sites of CCK-BCs at the PN soma, WT Nex1Cre-ERT2: Ank2$^{+/+}$: EGFP^{flox} mice (P21) were induced for EGFP expression (P10-P13) in cortical PNs. NrCAM (magenta) and EGFP (green) immunostaining was carried out and analyzed in PFC layer 2/3. Confocal imaging showed co-localization of NrCAM at the perisomatic region of EGFP+ PNs (Fig. 6A). Discrete synaptic puncta co-labeled for both NrCAM and EGFP were difficult to resolve, however NrCAM+ processes could be seen and some were adjacent to EGFP+ PN soma. To ask if NrCAM was also localized on presynaptic CCK-BCs during postnatal development, brain sections from Sncg-IRES2-tdT mice (P21) were immunostained for NrCAM (magenta) and tdT (green) then imaged confocally. NrCAM immunoreactivity was prominent at soma of tdT+ basket cells, labeled with antibodies to mCherry (Fig. 6 B). NrCAM immunoreactivity was also observed in mCherry+ neuronal processes.

In addition NrCAM was expressed by nearly all GFAP+ astrocytes (94% ± 0.01; n=387 GFAP+ cells) in the PFC of Sncg-IRES2-tdT mice at P21 (Fig. 6 C). NCAM localization to astrocytes was previously described in other brain regions [22]. NrCAM was also expressed by a subpopulation of parvalbumin-positive basket cells in this region (58% ± 0.01; n=112 PV+ cells), as shown by double labeling with NrCAM and parvalbumin antibodies (Fig. 6 D).

Taken together these results were consistent with possible pre- and post-synaptic homophilic binding role for NrCAM in perisomatic synapse formation between CCK-BCs and PNs, in addition to astrocytic NrCAM contact in tripartite synapse development..

4. Discussion

Here we show that NrCAM and its binding partner AnkB are required for synaptic contacts formed by VGlut3-expressing CCK-BCs with the perisomatic domain of PNs in the mouse PFC. A significant decrease was observed in the

number of VGlut3+ CCK-BC synaptic puncta on PN soma in PFC layer 2/3 of NrCAM-null and AnkB conditional mutant mice compared to WT. This decrease in synaptic puncta was specific for perisomatic targeting of VGlut3+ CCK-BCs, as NrCAM- or AnkB deletion did not alter the density of Syt2B+ perisomatic synaptic contacts made by PV-BCs onto PNs. NrCAM deletion did not decrease the density of VGlut3+ synaptic contacts made by CCK-BCs onto PV-BCs, and did not result in loss of these neurons. NrCAM was expressed by CCK-BCs and PNs postnatally consistent with a pre- and postsynaptic role for NrCAM-Ankyrin B in formation or stabilization of inhibitory connectivity between CCK-BCs and principal excitatory neurons in the PFC.

Proteomic studies identified NrCAM as a neuronal adhesion molecule necessary for GABAergic inhibitory synapse formation in mouse brain [21, 22]. However these reports did not identify the interneuron cell type dependent on NrCAM or the subcellular compartment of synaptic targeting. Results shown here support the conclusion that NrCAM mediates perisomatic synaptic connectivity between cortical PNs and CCK-BCs but not with PV-BCs. This finding is in accord with functional studies showing that NrCAM knockdown in astrocytes increases the rise time of mIPSCs suggesting inhibitory regulation at the somatic compartment rather than distal dendritic sites. The present work demonstrates localization of NrCAM on Sncg+/CCK-BCs, PN soma, and astrocytes. The NrCAM expression pattern is in line with homophilic NrCAM interactions between CCK-BC axons and PN soma, in addition to astroglia, potentially promoting tripartite neuronal-glial contacts important for synaptogenesis [22].

NrCAM and other members of the L1 family of homophilic adhesion molecules have a consensus binding site (FIGQY) for Ankyrins in their cytoplasmic domain. Conditional deletion of AnkB from postmitotic PNs at early postnatal stages (P10-P13) impaired perisomatic synaptic targeting of VGlut3+ CCK-BC inputs in Nex1Cre-ERT2: Ank2$^{flox/flox}$: EGFP^{flox} mice but did not alter the number of Syt2B+ PV-BC inputs. This time frame coincided with postnatal development of GAD65 perisomatic synaptic puncta, which increase from P10 to P21 and plateau at P60 in the PFC [35]. A postsynaptic role for NrCAM on PN

soma is supported by the finding that NrCAM binds the inhibitory postsynaptic scaffold protein gephyrin [21]. AnkB also localizes preferentially to the PN somatodendritic compartment [18]. Therefore, AnkB recruitment to NrCAM in PN soma may serve to stabilize CCK-BC inputs. Similarly, the AnkB binding site on L1 (FIGQY) promotes GABAergic synaptogenesis on PN soma in the PFC [35]. L1 was shown to drive chandelier interneuron innervation of the PN axon initial segment requiring anchoring by Ankyrin G [40]. It is interesting to speculate that AnkB binding to L1 or CHL1 might promote perisomatic synaptic contacts made by PV-BCs.

A limitation is that NrCAM deletion in null mutant mice affects expression in CCK-BCs, PNs, and astroglia, thus effects on CCK-BC synapses cannot be ascribed to a particular cell type. However, NrCAM in neurons clearly contributes to synaptogenesis since Takano et al., [22] showed that NrCAM knockdown in neurons using the neuronal promoter Synapsin I decreased the numbers of inhibitory synaptic contacts. It is therefore reasonable to expect that homophilic NrCAM binding between CCK-BCs and PNs, and possibly between neurons and glia, cooperate to form tripartite synaptic sites necessary for synaptogenesis.

Exploiting a new transgenic mouse line Sncg-IRES-FlpO: tdTomato, which specifically labels a population of VGlut3-expressing CCK-BCs in the cortex and hippocampus/dentate gyrus, we were able to validate NrCAM expression during synaptogenesis of CCK-BCs. Colocalization experiments with this reporter line demonstrated that NrCAM was expressed postnatally by Sncg+ CCK-BCs , where it localized to soma and processes, as well as in astrocytes. In Nex1Cre-ERT2: Ank2$^{+/+}$: EGFP^{flox} mice NrCAM localized to PN soma and apical dendrites. Thus NrCAM in pre- and postsynaptic neurons, and in astroglia is in position to play a homophilic adhesive role in perisomatic synaptogenesis of CCK-BCs. However, other synaptic molecules such as dystroglycan also contribute to perisomatic targeting of CCK-BCs [41]. SCNG-IRES-FlpO; tdT mice will help advance our knowledge of CCK-BCs, which has been limited by differences in expression in other lines that target CCK-BCs, including CCK-Cre [42, 7], VGlut3-Cre [43], cannabinoid-1 receptor Cre [44] mice .

5. Conclusion

The findings of this study demonstrate a role for NrCAM and its binding partner Ankyrin B in development of inhibitory connectivity between a VGlut3-expressing CCK-BCs and layer 2/3 PNs in the mouse PFC. Deletion of NrCAM in null mutant mice resulted in decreased numbers of VGlut3+ CCK-BC synaptic contacts in PFC layer 2/3, which may affect circuits whose disruption results in behavioral deficits in sociability, reversal learning, and addiction vulnerability observed in NrCAM-null mice [20, 45]. It has been suggested that cortical microcircuits in ASD are associated with an increased ratio of excitatory/inhibitory synapses that results in hyperexcitability [46, 47]. Deficiencies in NrCAM and the high confidence ASD risk factor AnkB may contribute to excitatory/inhibitory imbalance by diminishing inhibitory connectivity between CCK-BCs and principal excitatory neurons in the PFC affecting cognitive and social behaviors relevant to ASD.

Abbreviations: CCK-BCs, cholecystokinin-expressing basket cells; PNs, pyramidal neurons; Sncg, Synuclein-γ; PV, parvalbumin; vGlut3, vesicular glutamate transporter 3; Syt2, synaptotagmin-2; tdT, tdTomato.

Acknowledgements

We thank Erin Zhang and Ernest Pereira for expert assistance with the experiments. Dr. Paul Manis is gratefully acknowledged for microscopy of intrinsic fluorescence in the reporter mouse line. Dr. Pablo Ariel, Director of the UNC Microscopy Services Laboratory (MSL) in the Departments of Pathology and Laboratory Medicine, provided advice and assistance with confocal mioroscopy. Dr. Bryce Duncan (UNC) kindly provided help with EVOS microscopy.

Funding Sources

Support for this work was provided by National Institutes of Health grant R01 MH113280 (P.F.M.) and NIH Cancer Center Core Grant P30CA016086 (UNC MSL).

References

1. Forrest M. P., Parnell E., Penzes P. (2018) Dendritic Structural Plasticity and Neuropsychiatric Disease. Nat Rev Neurosci 19:215-234.
2. Freund T. F., Katona I. (2007) Perisomatic Inhibition. Neuron 56:33-42.
3. Bartos M., Elgueta C. (2012) Functional Characteristics of Parvalbumin- and Cholecystokinin-Expressing Basket Cells. J Physiol 590:669-681.
4. Armstrong C., Soltesz I. (2012) Basket Cell Dichotomy in Microcircuit Function. J Physiol 590:683-694.
5. Hu H., Gan J., Jonas P. (2014) Interneurons. Fast-Spiking, Parvalbumin(+) Gabaergic Interneurons: From Cellular Design to Microcircuit Function. Science 345:1255263.
6. Del Pino I., Brotons-Mas J. R., Marques-Smith A., Marighetto A., Frick A., Marin O., Rico B. (2017) Abnormal Wiring of Cck(+) Basket Cells Disrupts Spatial Information Coding. Nat Neurosci 20:784-792.
7. Nguyen R., Venkatesan S., Binko M., Bang J. Y., Cajanding J. D., Briggs C., Sargin D., Imayoshi I., Lambe E. K., Kim J. C. (2020) Cholecystokinin-Expressing Interneurons of the Medial Prefrontal Cortex Mediate Working Memory Retrieval. J Neurosci 40:2314-2331.
8. Goldman-Rakic P. S. (1995) Architecture of the Prefrontal Cortex and the Central Executive. Ann N Y Acad Sci 769:71-83.
9. Yizhar O., Fenno L. E., Prigge M., Schneider F., Davidson T. J., O'shea D. J., Sohal V. S., Goshen I., Finkelstein J., Paz J. T., Stehfest K., Fudim R., Ramakrishnan C., Huguenard J. R., Hegemann P., Deisseroth K. (2011) Neocortical Excitation/Inhibition Balance in Information Processing and Social Dysfunction. Nature 477:171-178.
10. Bastos A. M., Loonis R., Kornblith S., Lundqvist M., Miller E. K. (2018) Laminar Recordings in Frontal Cortex Suggest Distinct Layers for Maintenance and Control of Working Memory. Proc Natl Acad Sci U S A 115:1117-1122.

11. Quiquempoix M., Fayad S. L., Boutourlinsky K., Leresche N., Lambert R. C., Bessaih T. (2018) Layer 2/3 Pyramidal Neurons Control the Gain of Cortical Output. Cell Rep 24:2799-2807.
12. Fortier A. V., Meisner O. C., Nair A. R., Chang S. W. C. (2022) Prefrontal Circuits Guiding Social Preference: Implications in Autism Spectrum Disorder. Neurosci Biobehav Rev 141:104803.
13. Whissell P. D., Cajanding J. D., Fogel N., Kim J. C. (2015) Comparative Density of Cck- and Pv-Gaba Cells within the Cortex and Hippocampus. Front Neuroanat 9:124.
14. Maness P. F., Schachner M. (2007) Neural Recognition Molecules of the Immunoglobulin Superfamily: Signaling Transducers of Axon Guidance and Neuronal Migration. Nat Neurosci 10:19-26.
15. Mohan V., Sullivan C. S., Guo J., Wade S. D., Majumder S., Agarwal A., Anton E. S., Temple B. S., Maness P. F. (2019) Temporal Regulation of Dendritic Spines through Nrcam-Semaphorin3f Receptor Signaling in Developing Cortical Pyramidal Neurons. Cereb Cortex 29:963-977.
16. Duncan B. W., Mohan V., Wade S. D., Truong Y., Kampov-Polevoi A., Temple B. R., Maness P. F. (2021) Semaphorin3f Drives Dendritic Spine Pruning through Rho-Gtpase Signaling. Mol Neurobiol 58:3817-3834.
17. Demyanenko G. P., Mohan V., Zhang X., Brennaman L. H., Dharbal K. E., Tran T. S., Manis P. B., Maness P. F. (2014) Neural Cell Adhesion Molecule Nrcam Regulates Semaphorin 3f-Induced Dendritic Spine Remodeling. J Neurosci 34:11274-11287.
18. Nelson A. D., Catalfio A. M., Gupta J. P., Min L., Caballero-Floran R. N., Dean K. P., Elvira C. C., Derderian K. D., Kyoung H., Sahagun A., Sanders S. J., Bender K. J., Jenkins P. M. (2024) Physical and Functional Convergence of the Autism Risk Genes Scn2a and Ank2 in Neocortical Pyramidal Cell Dendrites. Neuron.
19. Marui T., Funatogawa I., Koishi S., Yamamoto K., Matsumoto H., Hashimoto O., Nanba E., Nishida H., Sugiyama T., Kasai K., Watanabe K., Kano Y., Sasaki T., Kato N. (2009) Association of the Neuronal Cell

Adhesion Molecule (Nrcam) Gene Variants with Autism. Int J Neuropsychopharmacol 12:1-10.

20. Moy S. S., Nonneman R. J., Young N. B., Demyanenko G. P., Maness P. F. (2009) Impaired Sociability and Cognitive Function in Nrcam-Null Mice. Behav Brain Res 205:123-131.
21. Uezu A., Kanak D. J., Bradshaw T. W., Soderblom E. J., Catavero C. M., Burette A. C., Weinberg R. J., Soderling S. H. (2016) Identification of an Elaborate Complex Mediating Postsynaptic Inhibition. Science 353:1123-1129.
22. Takano T., Wallace J. T., Baldwin K. T., Purkey A. M., Uezu A., Courtland J. L., Soderblom E. J., Shimogori T., Maness P. F., Eroglu C., Soderling S. H. (2020) Chemico-Genetic Discovery of Astrocytic Control of Inhibition in Vivo. Nature 588:296-302.
23. Anastasiades P. G., Carter A. G. (2021) Circuit Organization of the Rodent Medial Prefrontal Cortex. Trends Neurosci 44:550-563.
24. Sakurai T., Lustig M., Babiarz J., Furley A. J., Tait S., Brophy P. J., Brown S. A., Brown L. Y., Mason C. A., Grumet M. (2001) Overlapping Functions of the Cell Adhesion Molecules Nr-Cam and L1 in Cerebellar Granule Cell Development. J Cell Biol 154:1259-1273.
25. Murphy K. E., Duncan B., Sperringer J. E., Zhang E., Haberman V., Wyatt E. V., Maness P. (2023) Ankyrin B Promotes Developmental Spine Regulation in the Mouse Prefrontal Cortex. Cereb Cortex 33:10634-10648.
26. Agarwal A., Dibaj P., Kassmann C. M., Goebbels S., Nave K. A., Schwab M. H. (2012) In Vivo Imaging and Noninvasive Ablation of Pyramidal Neurons in Adult Nex-Creert2 Mice. Cereb Cortex 22:1473-1486.
27. Madisen L., Garner A. R., Shimaoka D., Chuong A. S., Klapoetke N. C., Li L., Van Der Bourg A., Niino Y., Egolf L., Monetti C., Gu H., Mills M., Cheng A., Tasic B., Nguyen T. N., Sunkin S. M., Benucci A., Nagy A., Miyawaki A., Helmchen F. et al. (2015) Transgenic Mice for Intersectional Targeting of Neural Sensors and Effectors with High Specificity and Performance. Neuron 85:942-958.

28. Daigle T. L., Madisen L., Hage T. A., Valley M. T., Knoblich U., Larsen R. S., Takeno M. M., Huang L., Gu H., Larsen R., Mills M., Bosma-Moody A., Siverts L. A., Walker M., Graybuck L. T., Yao Z., Fong O., Nguyen T. N., Garren E., Lenz G. H. et al. (2018) A Suite of Transgenic Driver and Reporter Mouse Lines with Enhanced Brain-Cell-Type Targeting and Functionality. Cell 174:465-480 e422.
29. Somogyi J., Baude A., Omori Y., Shimizu H., El Mestikawy S., Fukaya M., Shigemoto R., Watanabe M., Somogyi P. (2004) Gabaergic Basket Cells Expressing Cholecystokinin Contain Vesicular Glutamate Transporter Type 3 (Vglut3) in Their Synaptic Terminals in Hippocampus and Isocortex of the Rat. Eur J Neurosci 19:552-569.
30. Miczan V., Kelemen K., Glavinics J. R., Laszlo Z. I., Barti B., Kenesei K., Kisfali M., Katona I. (2021) Necab1 and Necab2 Are Prevalent Calcium-Binding Proteins of Cb1/Cck-Positive Gabaergic Interneurons. Cereb Cortex 31:1786-1806.
31. Sugita S., Ho A., Sudhof T. C. (2002) Necabs: A Family of Neuronal Ca(2+)-Binding Proteins with an Unusual Domain Structure and a Restricted Expression Pattern. Neuroscience 112:51-63.
32. Sommeijer J. P., Levelt C. N. (2012) Synaptotagmin-2 Is a Reliable Marker for Parvalbumin Positive Inhibitory Boutons in the Mouse Visual Cortex. PLoS One 7:e35323.
33. Karson M. A., Tang A. H., Milner T. A., Alger B. E. (2009) Synaptic Cross Talk between Perisomatic-Targeting Interneuron Classes Expressing Cholecystokinin and Parvalbumin in Hippocampus. J Neurosci 29:4140-4154.
34. Bennett V., Healy J. (2009) Membrane Domains Based on Ankyrin and Spectrin Associated with Cell-Cell Interactions. Cold Spring Harb Perspect Biol 1:1-19.
35. Guan H., Maness P. F. (2010) Perisomatic Gabaergic Innervation in Prefrontal Cortex Is Regulated by Ankyrin Interaction with the L1 Cell Adhesion Molecule. Cereb Cortex 20:2684-2693.

36. Tseng W. C., Jenkins P. M., Tanaka M., Mooney R., Bennett V. (2015) Giant Ankyrin-G Stabilizes Somatodendritic Gabaergic Synapses through Opposing Endocytosis of Gabaa Receptors. Proc Natl Acad Sci U S A 112:1214-1219.
37. Tasic B., Menon V., Nguyen T. N., Kim T. K., Jarsky T., Yao Z., Levi B., Gray L. T., Sorensen S. A., Dolbeare T., Bertagnolli D., Goldy J., Shapovalova N., Parry S., Lee C., Smith K., Bernard A., Madisen L., Sunkin S. M., Hawrylycz M. et al. (2016) Adult Mouse Cortical Cell Taxonomy Revealed by Single Cell Transcriptomics. Nat Neurosci 19:335-346.
38. Dudok B., Szoboszlay M., Paul A., Klein P. M., Liao Z., Hwaun E., Szabo G. G., Geiller T., Vancura B., Wang B. S., Mckenzie S., Homidan J., Klaver L. M. F., English D. F., Huang Z. J., Buzsaki G., Losonczy A., Soltesz I. (2021) Recruitment and Inhibitory Action of Hippocampal Axo-Axonic Cells During Behavior. Neuron 109:3838-3850 e3838.
39. Dudok B., Klein P. M., Hwaun E., Lee B. R., Yao Z., Fong O., Bowler J. C., Terada S., Sparks F. T., Szabo G. G., Farrell J. S., Berg J., Daigle T. L., Tasic B., Dimidschstein J., Fishell G., Losonczy A., Zeng H., Soltesz I. (2021) Alternating Sources of Perisomatic Inhibition During Behavior. Neuron 109:997-1012.
40. Tai Y., Gallo N. B., Wang M., Yu J. R., Van Aelst L. (2019) Axo-Axonic Innervation of Neocortical Pyramidal Neurons by Gabaergic Chandelier Cells Requires Ankyring-Associated L1cam. Neuron 102:358-372.
41. Miller D. S., Wright K. M. (2021) Neuronal Dystroglycan Regulates Postnatal Development of Cck/Cannabinoid Receptor-1 Interneurons. Neural Dev 16:4.
42. Taniguchi H., He M., Wu P., Kim S., Paik R., Sugino K., Kvitsiani D., Fu Y., Lu J., Lin Y., Miyoshi G., Shima Y., Fishell G., Nelson S. B., Huang Z. J. (2011) A Resource of Cre Driver Lines for Genetic Targeting of Gabaergic Neurons in Cerebral Cortex. Neuron 71:995-1013.

43. Pelkey K. A., Calvigioni D., Fang C., Vargish G., Ekins T., Auville K., Wester J. C., Lai M., Mackenzie-Gray Scott C., Yuan X., Hunt S., Abebe D., Xu Q., Dimidschstein J., Fishell G., Chittajallu R., Mcbain C. J. (2020) Paradoxical Network Excitation by Glutamate Release from Vglut3(+) Gabaergic Interneurons. Elife 9.
44. Marsicano G., Wotjak C. T., Azad S. C., Bisogno T., Rammes G., Cascio M. G., Hermann H., Tang J., Hofmann C., Zieglgansberger W., Di Marzo V., Lutz B. (2002) The Endogenous Cannabinoid System Controls Extinction of Aversive Memories. Nature 418:530-534.
45. Ishiguro H., Hall F. S., Horiuchi Y., Sakurai T., Hishimoto A., Grumet M., Uhl G. R., Onaivi E. S., Arinami T. (2012) Nrcam-Regulating Neural Systems and Addiction-Related Behaviors. Addict Biol.
46. Rubenstein J. L., Merzenich M. M. (2003) Model of Autism: Increased Ratio of Excitation/Inhibition in Key Neural Systems. Genes Brain Behav 2:255-267.
47. Zikopoulos B., Barbas H. (2010) Changes in Prefrontal Axons May Disrupt the Network in Autism. J Neurosci 30:14595-14609.

Figure Legends

Figure 1. CCK-basket cell synaptic puncta on soma of cortical pyramidal neurons (PNs) are decreased in PFC of adult NrCAM-null mutant mice.

A. PNs in PFC layer 2/3 of WT and NrCAM-null mice were immunostained for somal marker MATH2 (green). CCK-BC presynaptic puncta on PN soma were immunostained for VGlut3 (red, white arrowheads). Confocal images show a representative maximum intensity projection of 5 optical sections (~0.3 µm each) (bars = 20 µm). Inserts show higher magnifications of PN soma (bars = 5 µm).
B. Quantification of VGluT3+ synaptic puncta per MATH2+ PN soma in WT and NrCAM-null PFC . Data points represent the average number of puncta per soma per image. Mean number of puncta per soma were significantly different between genotypes (two tailed t-test: p* = 0.01).
C. PNs were immunostained for MATH2 (blue) and perisomatic puncta from CCK-BCs and PV-BCs were immunostained for VGAT (red, white arrowheads) in WT and NrCAM-null mice (bars = 20 µm). Representative confocal images as described in A are shown. Inserts show higher magnification of PN soma (bars = 5 µm).
D. Quantification of VGAT+ synaptic puncta per MATH2+ PN soma in WT and NrCAM-null PFC. Data points represent the mean number of puncta per soma per image. Mean number of puncta per soma were significantly different between genotypes (two tailed t-test: *p = 0.02).
E. Immunostaining of CCK-BC marker NECAB1 (white, arrowheads) in WT and NrCAM-null PFC. Representative nonconfocal images from EVOS microscopy. Bar =100 µm.
F. Quantification of mean NECAB1+ soma per mm^2 in nonconfocal EVOS images. Differences between WT and NrCAM-null genotypes were not significant by two tailed t-test: p = 0.99 (ns).

Figure 2. Perisomatic synaptic puncta from PV-BCs onto PN soma are not decreased in PFC of NrCAM-null mutant PFC.

A. Immunofluorescent staining of Syt2B+ synaptic puncta (red, arrowheads) on MATH2+ PN soma (blue) in WT and NrCAM-null PFC layer 2/3. Representative confocal images are shown. Bars= 20 µm, cell insert 5 µm
B. Quantitation of Syt2b+ synaptic puncta per MATH2+ soma ($x10^{-1}$). Data points represent the average number of puncta per soma in each image. Mean numbers of puncta per soma between genotypes WT and NrCAM-null were not significant (ns) by two tailed t-test: $p = 0.08$.
C. Immunostaining of VGluT3+ CCK-BC synaptic puncta (red, arrowheads) on PV-BC soma immunostained for parvalbumin (blue). Representative confocal images are shown. Bars = 20 µm, cell insert 5 µm.
D. Quantitation of VGlut3+ synaptic puncta on PV-BC soma stained for parvalbumin (green). Data points represent the average number of puncta per soma per image. Mean numbers of VGluT3+ puncta per PV+ soma were not significantly different (ns) between WT and NrCAM-null genotypes (two tailed t-test: $p = 0.28$).

Figure 3. Perisomatic synaptic puncta from CCK-BCs onto PN soma are decreased in PFC of Nex1Cre-ERT2: Ank2+/+ (WT) and Ank2 F/F mice,

A. Immunofluorescent staining of VGluT3+ synaptic puncta (red, arrows) on EGFP+ PN soma (green) in Ank2+/+(WT) and Ank2 F/F mice (~P60) deleted for AnkB in postmitotic PNs. Confocal images show representative maximum intensity projections. Bars: 20 µm
B. Quantitation of VGlut3+ synaptic puncta on EGFP+ soma. Data points represent the average number of puncta per soma for each image ($n \geq 10$ images/case) in z-stacks through the soma. Mean number of puncta per soma for genotypes Ank2+/+ and Ank2 F/F were significant (two tailed t-test, $p < 0.0001$*).
C. Immunofluorescent staining of NECAB1+ soma on EGFP+ PN soma (arrows) in Ank2+/+ and Ank2 F/F mice deleted for AnkB in postmitotic PNs. Cells without arrows were NECAB1-negative. Bars: 20 µm

D. Quantitation of NECAB1+ EGFP+ soma/mm^2 ($x10^{-1}$). Data points represent the average number of puncta per soma for each image (n ≥ 10 images/case) in z-stacks. Mean differences between Ank2+/+ and Ank2 F/F genotypes were not significant (ns) (two-tailed t-test, p = 0.25.)
E. Immunofluorescent staining of Syt2b+ synaptic puncta (red, arrows) on EGFP+ PN soma (green). Bars: 20 µm
F. Quantitation of Syt2b+ puncta per EGFP+ soma ($x10^{-1}$). Data points represent the averages number of puncta per soma in each image. Mean differences between genotypes of Ank2+/+ and Ank2 F/F were not significant (ns) (two tailed t-test, p =0.99.)

Figure 4. Expression of tdTomato in the PFC and hippocampus of Sncg-IRES2-tdT adult Mice (P60)

A. Immunofluorescent staining of tdT with dsRed antibodies in representative confocal images showed labeled cells throughout the PFC with higher levels in layer 2/3. Cortical layers I-VI are indicated.
B. Control staining with secondary antibodies alone was low.
C. Higher magnification of tdT+ cells showed neuronal morphology with labeled soma and processes (arrows).
D. Intrinsic tdT fluorescence in PFC layer 2/3 neurons was lower but visible in soma and processes (arrows) without dsRed antibody staining. Representative image from wide-field fluorescence microscopy with a 555 nM LED and Semrock filter set for tdT/mCherry.
E. IImmunofluorescent staining of tdT with dsRed antibodies in the hippocampus showed labeled cells mostly evident in the stratum pyramidale (SP) of CA1, CA2, and CA3, with fewer cells in the stratum oriens (SO), stratum radiatum (SR), and stratum lacunosum-moleculare (SLM). tdT+ cells were also observed in the dentate gyrus (DG) granule cell layer (GCL) and hilus (Hi).
F. Control staining with secondary antibodies alone was low.

G. Higher magnification of tdT+ cells in the SP showed neuronal morphology with labeled soma and processes (arrows).
H. Intrinsic tdT fluorescence in soma of SP neurons was lower but visible without dsRed antibody staining (arrows).

Figure 5. NECAB1-expression in tdT+ but not Parvalbumin+ interneurons in PFC

of Sncg-IRES2-tdT Mice

A. Double immunofluorescence staining for NECAB1 (magenta) and tdT using mCherry antibodies (green) showed that a subset (~25%) of mCherry+ neurons co-expressed NECAB1 in representative dual channel confocal images. Control staining with secondary antibodies alone was negative. (n=83 cells, 10 images, 3 mice).
B. Double immunofluorescence staining for Parvalbumin (PV; magenta) and tdTomato (anti-dsRed, green) indicated no detectable co-localization, as shown in representative dual channel merged confocal images. (n=156 cells, 10 images, 3 mice, 0 double labeled cells).
C. Time course of tdT expression at postnatal ages P34 (a), P42 (b), and P60 (c, d). Representative images of PFC layer 2/3 stained for tdTomato with dsRed antibodies or secondary antibody-only negative control.
D. Graph of cell density per mm2 by postnatal age. Anova with Tukey's post hoc analyses: P34 vs. P42: p = 0.005*; P34 vs P60: p = 0.0002*; P34-P60: p=0.072, not significant.

Figure 6. NrCAM expression in pyramidal neurons, CCK basket cells, and GFAP+ astrocytes in PFC of juvenile mice (P21).

A. Double Immunofluorescence staining for NrCAM (magenta) in Nex1Cre-ERT2: Ank2+/+;EGFP (WT) mice (P21) in soma of PNs expressing eGFP (green) in PFC layer 2/3. Negative control with secondary antibodies alone. Merged confocal image shows colocalization reflecting

postsynaptic localization of NrCAM on PN soma. Arrows point to NrCAM+ processes in proximity to EGFP+ PNs. Bar = 10 µm.

B. Double immunofluorescence staining for NrCAM (magenta) in tdT+ CCK-BCs of Sncg-IRES2-tdT mice (P21) labeled with mCherry antibodies (green) in PFC layer 2/3. Control with secondary antibodies alone was negative. Merged confocal image shows colocalization (arrows) reflecting NrCAM localization on presynaptic neurons. Bar = 10 µm.

C. Double Immunofluorescence staining for GFAP (green) and NrCAM (red) in tdT+ CCK-BCs of Sncg-IRES2-tdT mice (P21) in PFC layer 2/3. Merged confocal image shows colocalization of NrCAM in GFAP+ astrocytes.

D. Double Immunofluorescence staining for NrCAM (magenta) and parvalbumin (PV) (green) in CCK-BCs of Sncg-IRES2-tdT mice (P21) in PFC layer 2/3. Merged confocal image shows colocalization of NrCAM in GFAP+ astrocytes.

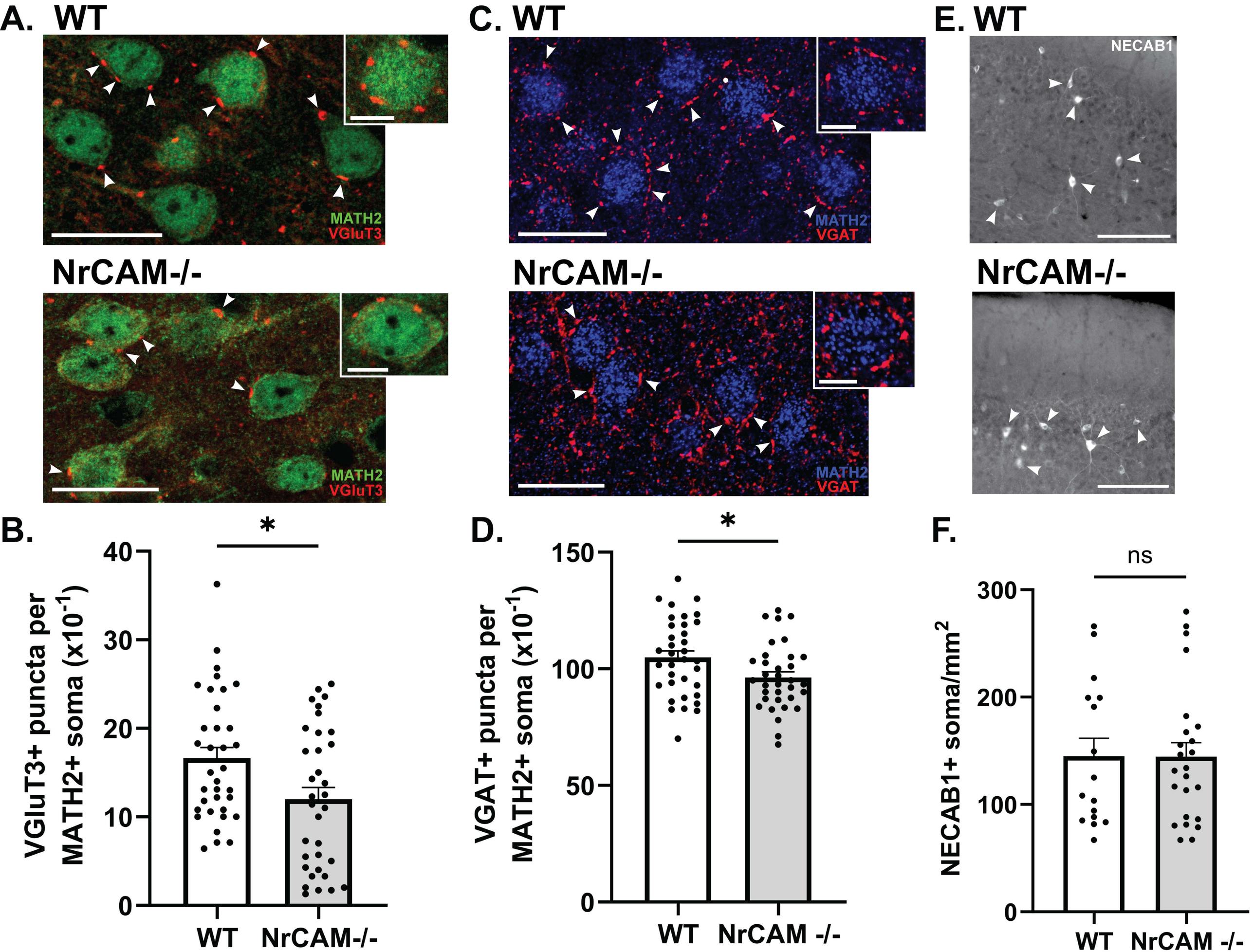
A. WT
MATH2
VGluT3
NrCAM-/-
MATH2
VGluT3
C. WT
MATH2
VGAT
NrCAM-/-
MATH2
VGAT
E. WT
NECAB1
NrCAM-/-
B.
*
VGluT3+ puncta per MATH2+ soma (x10-1)
40
30
20
10
0
WT
NrCAM-/-
D.
*
VGAT+ puncta per MATH2+ soma (x10-1)
150
100
50
0
WT
NrCAM -/-
F.
ns
NECAB1+ soma/mm2
300
200
100
0
WT
NrCAM -/-

A. WT

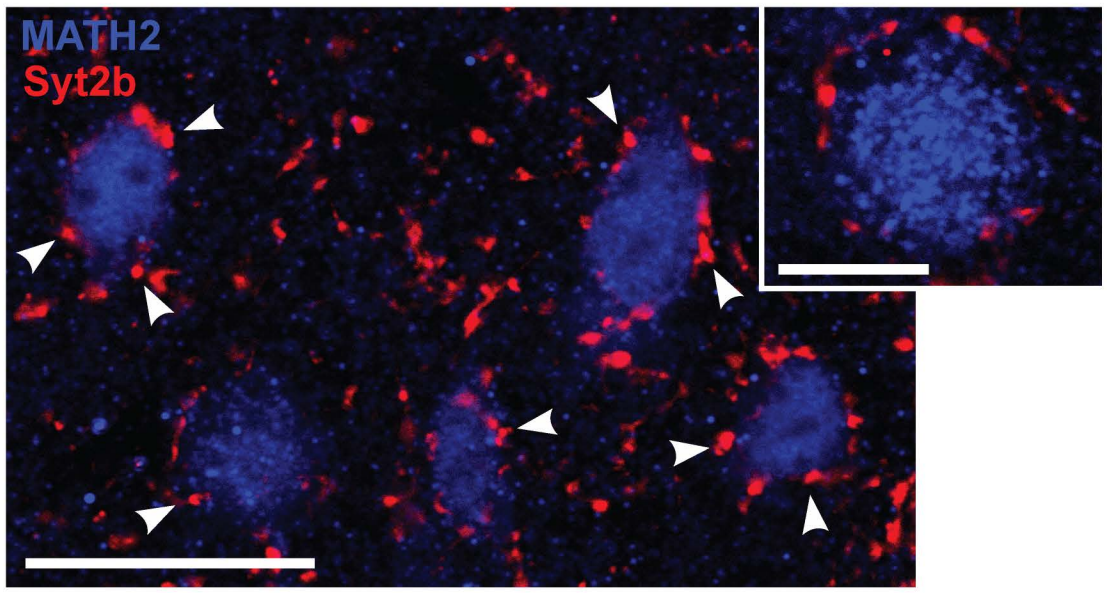

NrCAM-/-

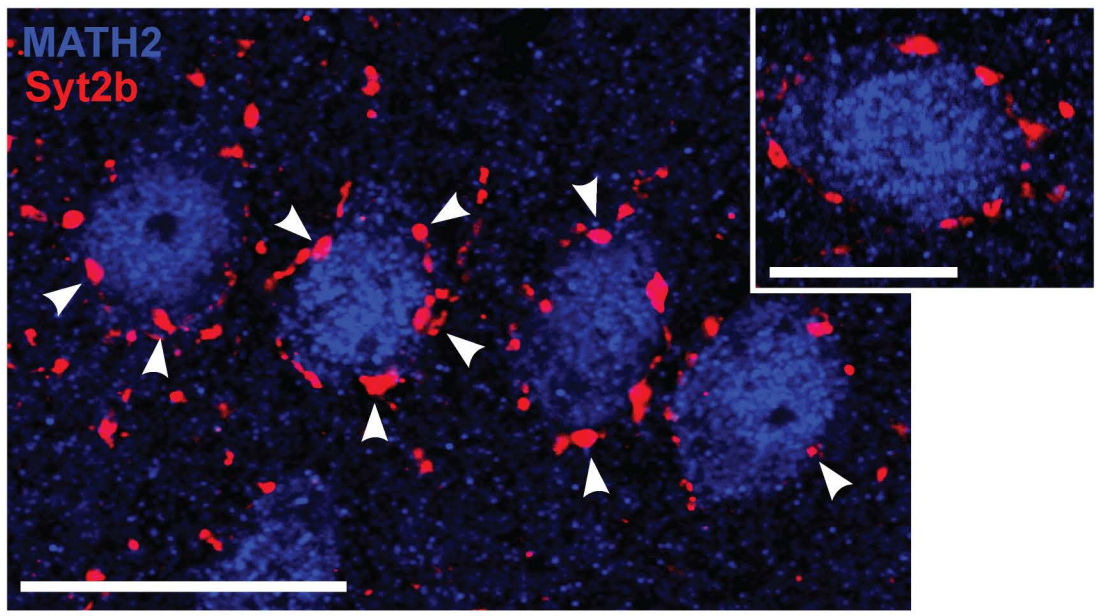

C. WT

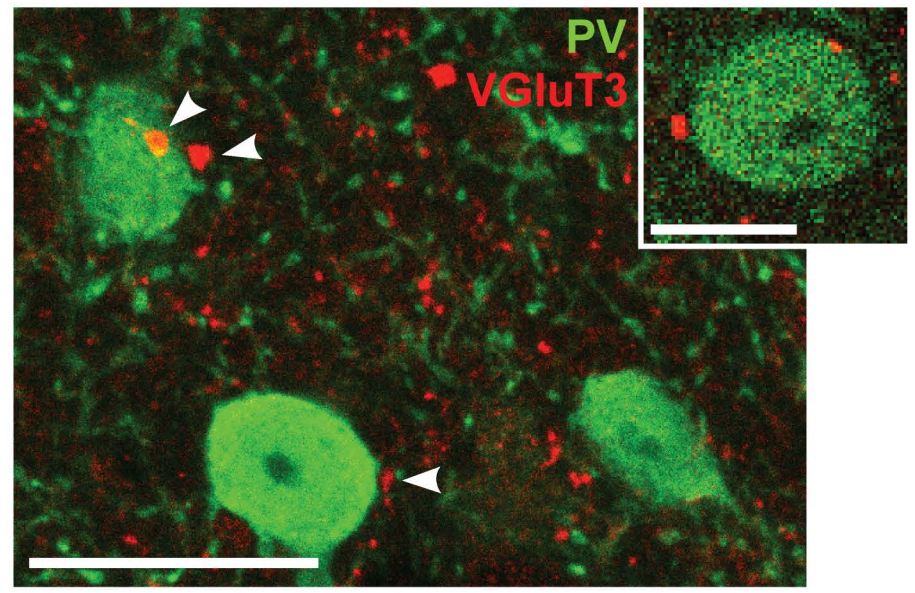

NrCAM-/-

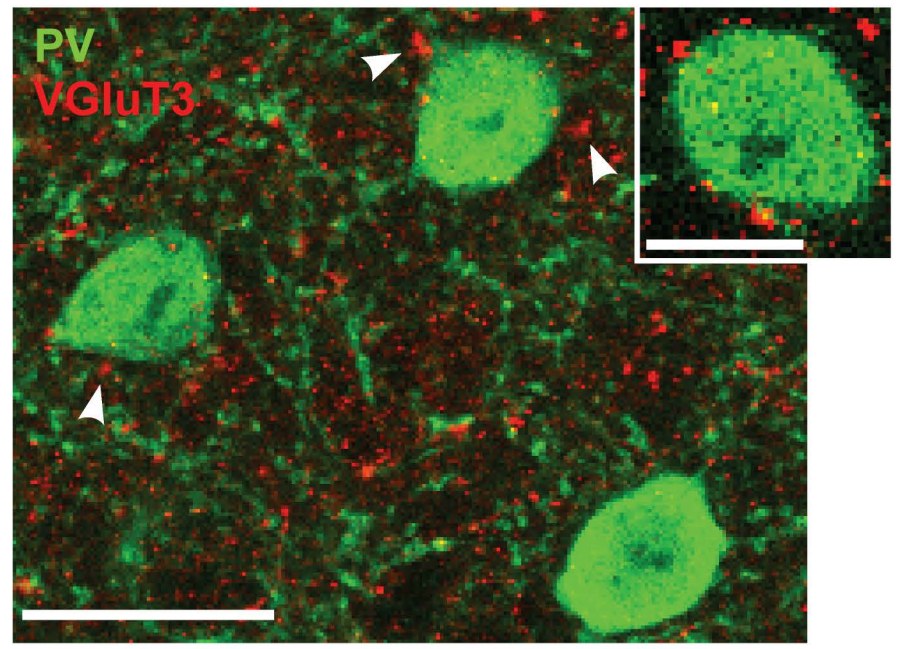

B.

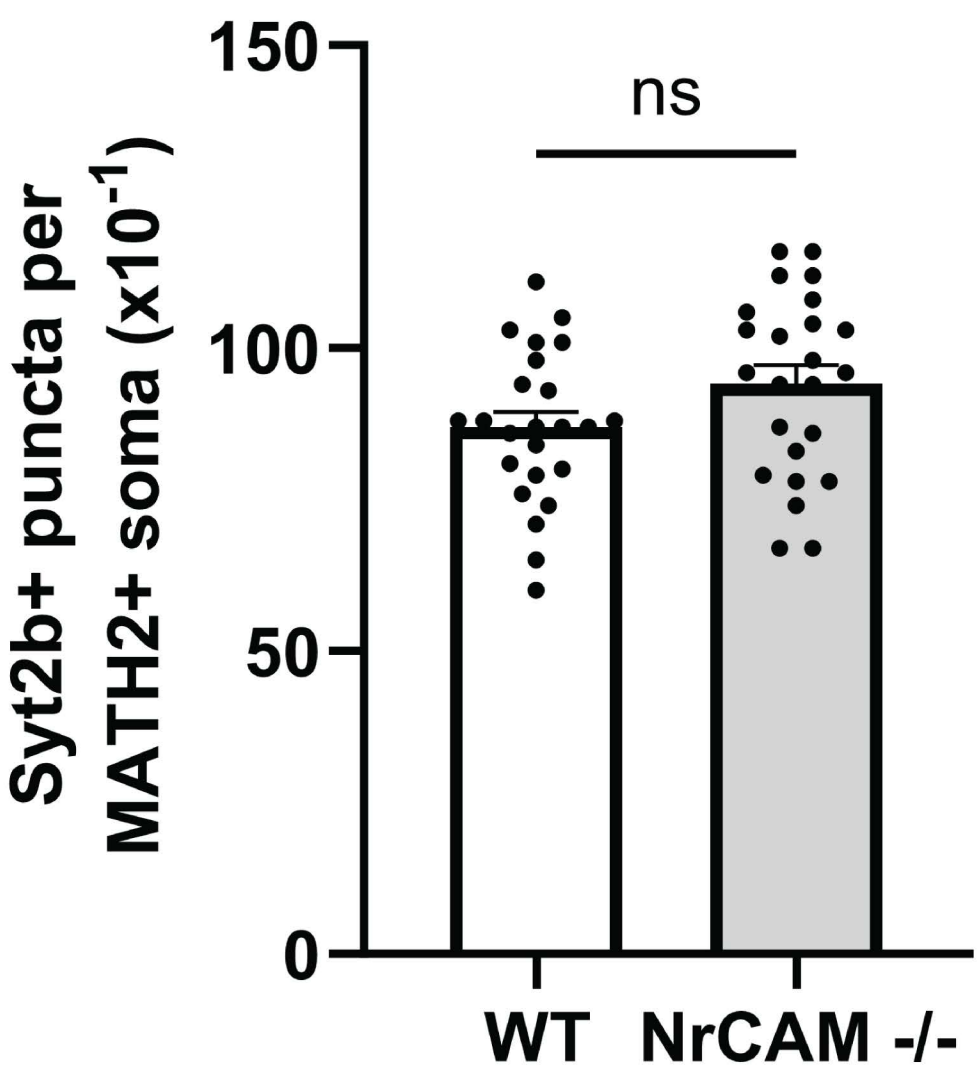

D.

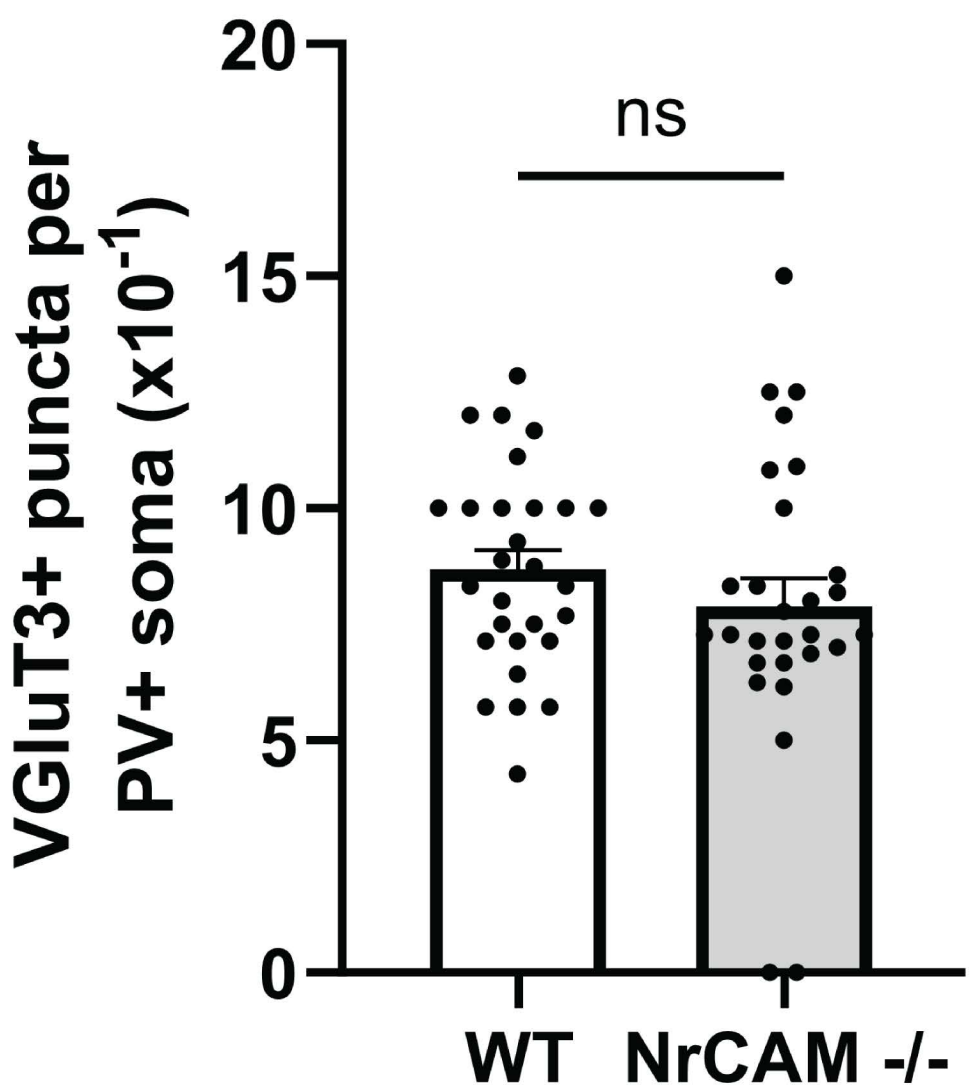

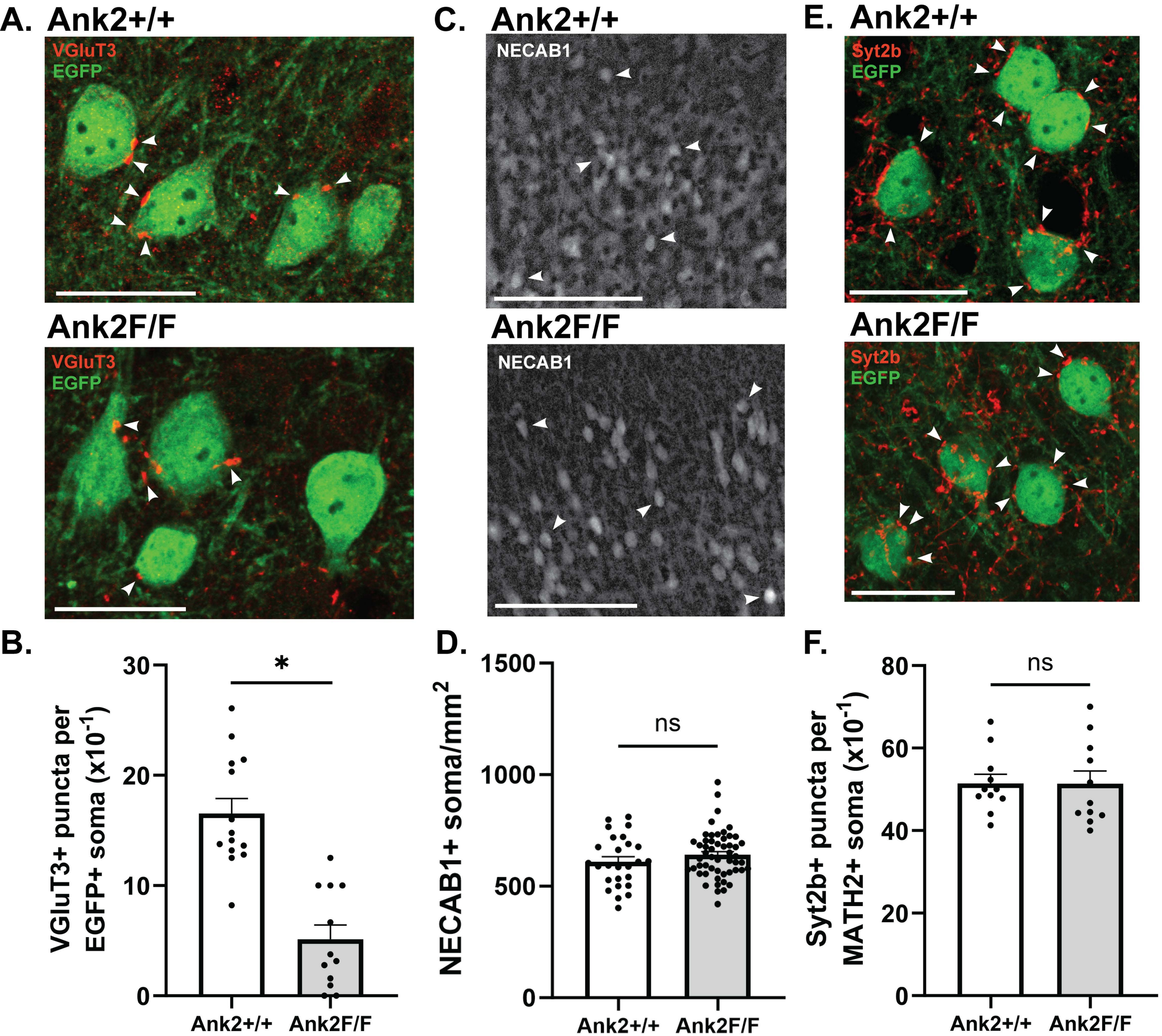
A.
Ank2+/+
VGluT3
EGFP
Ank2F/F
VGluT3
EGFP
C.
Ank2+/+
NECAB1
Ank2F/F
NECAB1
E.
Ank2+/+
Syt2b
EGFP
Ank2F/F
Syt2b
EGFP
B.
VGluT3+ puncta per EGFP+ soma (x10^-1)
30
20
10
0
*
Ank2+/+
Ank2F/F
D.
NECAB1+ soma/mm^2
1500
1000
500
0
ns
Ank2+/+
Ank2F/F
F.
Syt2b+ puncta per MATH2+ soma (x10^-1)
80
60
40
20
0
ns
Ank2+/+
Ank2F/F

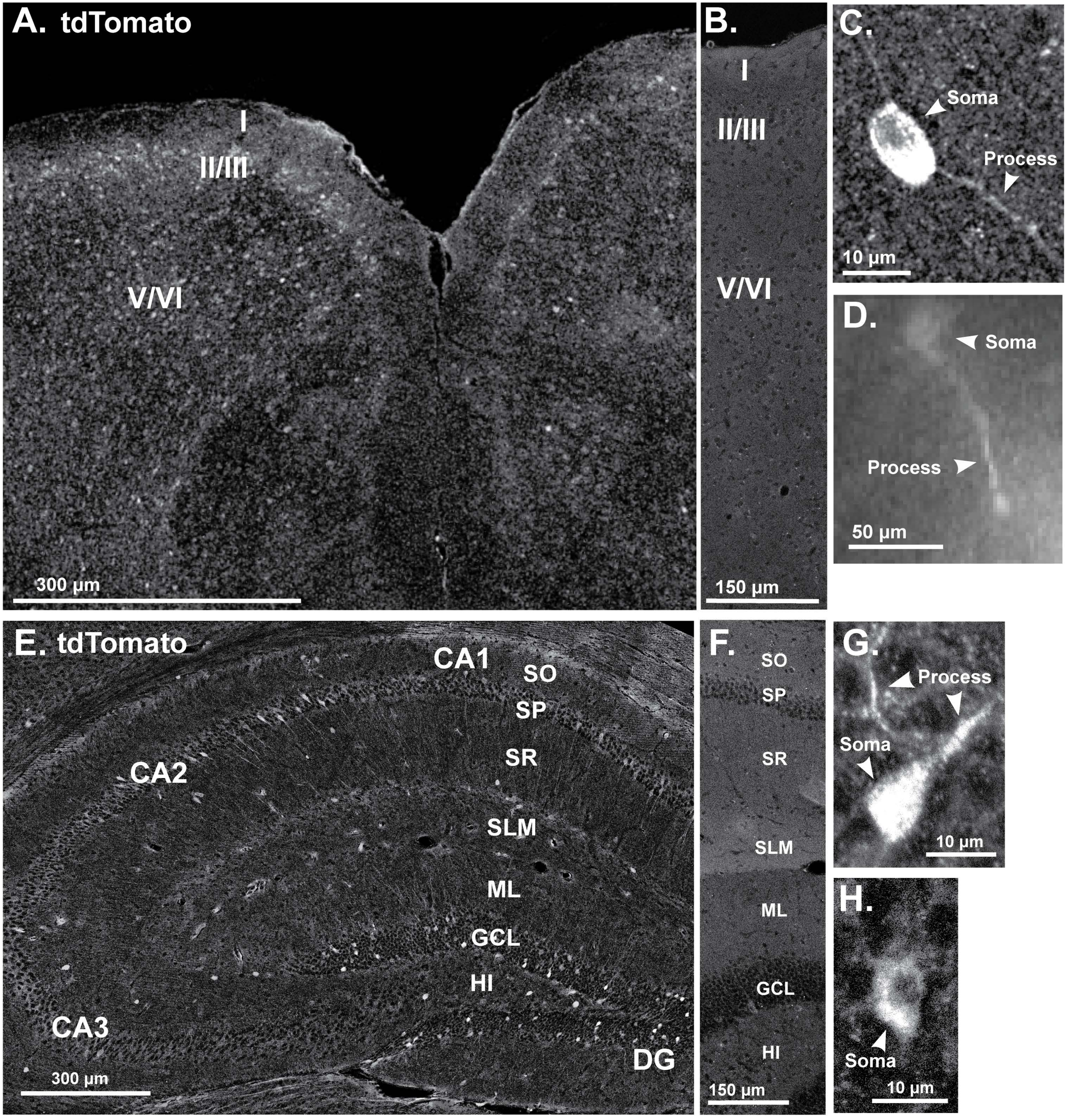
A. tdTomato
I
II/III
V/VI
300 µm
B.
I
II/III
V/VI
150 µm
C.
Soma
Process
10 µm
D.
Soma
Process
50 µm
E. tdTomato
CA1
SO
SP
SR
CA2
SLM
ML
GCL
HI
CA3
DG
300 µm
F.
SO
SP
SR
SLM
ML
GCL
HI
150 µm
G.
Process
Soma
10 µm
H.
Soma
10 µm

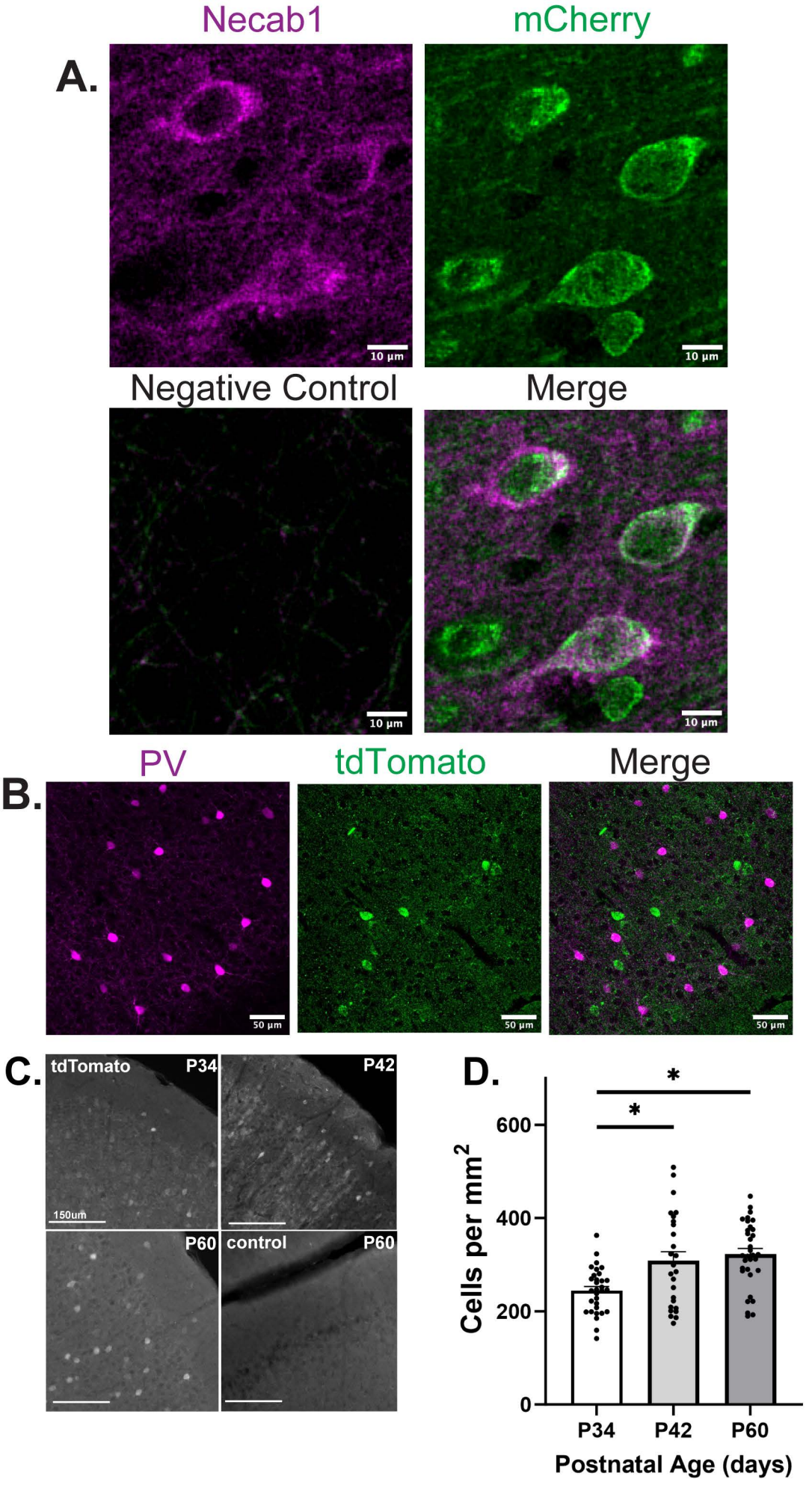
A.
Necab1
mCherry
10 µm
10 µm
Negative Control
Merge
10 µm
10 µm
B.
PV
tdTomato
Merge
50 µm
50 µm
50 µm
C.
tdTomato
P34
P42
150um
P60
control
P60
D.
Cells per mm2
600
400
200
0
*
*
P34
P42
P60
Postnatal Age (days)

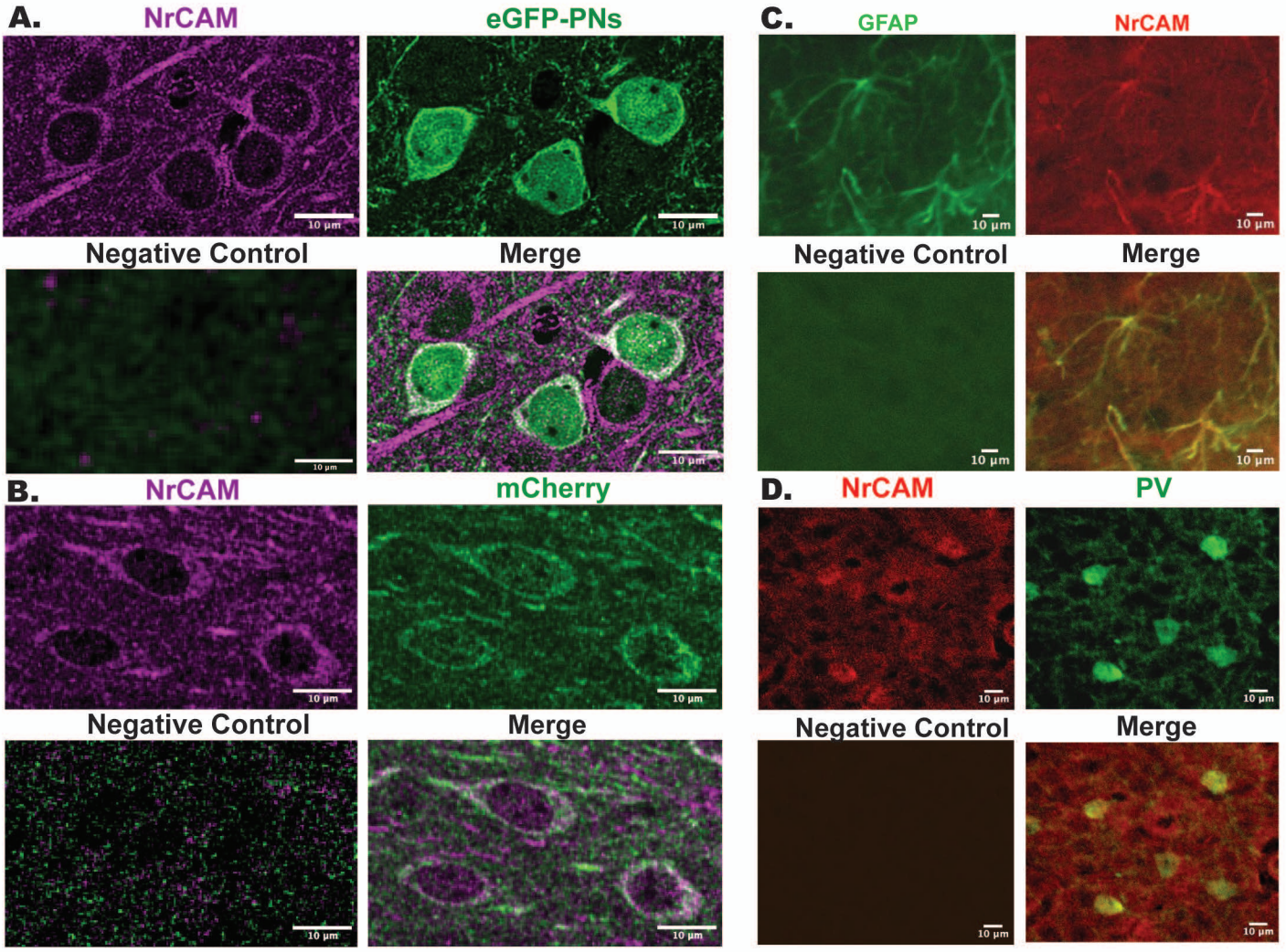
A.
NrCAM
eGFP-PNs
Negative Control
Merge
B.
NrCAM
mCherry
Negative Control
Merge
C.
GFAP
NrCAM
Negative Control
Merge
D.
NrCAM
PV
Negative Control
Merge
10 µm